

Enhancing the Electron Pair Approximation with Measurements on Trapped Ion Quantum Computers

Luning Zhao* and Joshua Goings
IonQ Inc, College Park, MD, 20740, USA

Qingfeng Wang
*Chemical Physics Program and Institute for Physical Science and Technology,
University of Maryland, College Park, MD, 20742, USA*

Kyuji Shin,[†] Woomin Kyoung, and Seunghyo Noh
*Materials Research & Engineering Center, CTO Division,
Hyundai Motor Company, Uiwang 16082, Republic of Korea*

Young Min Rhee and Kyungmin Kim
Department of Chemistry, KAIST, Daejeon, 34141, Republic of Korea
(Dated: December 12, 2023)

The electron pair approximation offers a resource efficient variational quantum eigensolver (VQE) approach for quantum chemistry simulations on quantum computers. With the number of entangling gates scaling quadratically with system size and a constant energy measurement overhead, the orbital optimized unitary pair coupled cluster double (oo-upCCD) ansatz strikes a balance between accuracy and efficiency on today's quantum computers. However, the electron pair approximation makes the method incapable of producing quantitatively accurate energy predictions. In order to improve the accuracy without increasing the circuit depth, we explore the idea of reduced density matrix (RDM) based second order perturbation theory (PT2) as an energetic correction to electron pair approximation. The new approach takes into account of the broken-pair energy contribution that is missing in pair-correlated electron simulations, while maintaining the computational advantages of oo-upCCD ansatz. In dissociations of N_2 , Li_2O , and chemical reactions such as the unimolecular decomposition of CH_2OH^+ and the S_N2 reaction of $CH_3I + Br^-$, the method significantly improves the accuracy of energy prediction. On two generations of the IonQ's trapped ion quantum computers, Aria and Forte, we find that unlike the VQE energy, the PT2 energy correction is highly noise-resilient. By applying a simple error mitigation approach based on post-selection solely on the VQE energies, the predicted VQE-PT2 energy differences between reactants, transition state, and products are in excellent agreement with noise-free simulators.

I. INTRODUCTION

Quantum computers have the potential to revolutionize a number of fields, including physical simulation,[1] optimization,[2] and machine learning.[3] Of particular interest is to solve the electronic structure problem of molecules and materials using quantum computers. It is well known that classically computing exact solutions to the electronic structure problem requires computational resources that grow exponentially with system size. To mitigate this problem, the current state of the art is to use polynomial scaling approximate methods to predict electronic properties. One example is the "gold standard" of electronic structure theory, projected coupled-cluster theory[4], namely CCSD(T).

In contrast, quantum algorithms unlock the potential to solve the *exact* electronic structure problem to arbitrary accuracy in polynomial space and time. Unfortunately, known algorithms with robust theoretical guarantees (such as phase estimation) remain highly sensitive to noise, and therefore require the use of fault-tolerant quantum computers with error corrections. Fault-tolerant quantum devices are likely many years away, so in the interim much effort has been made

to find algorithms that are noise-robust but still provide accurate solutions to electronic properties. The ultimate goal is to enable reliable predictions of energetics, geometries, binding affinities, response properties, and more. The reason for this is that access to robust and dependable predictions promises to greatly aid the development of functional materials,[5] next-generation battery,[6] drug discovery,[7] and novel catalysts.[8] Therefore, the potential advantage of quantum computers in this field is significant.

In recent years, significant progress has been made in quantum technologies, marked by advancements in both algorithmic methods and hardware capabilities. Presently, a variety of cloud-based quantum computing platforms are available, offering access to quantum processors with diverse architectures. These platforms, provided by several commercial cloud vendors, offer a variety of computational capacities, allowing the user to choose between systems with varying qubit connectivities, gate operation times, fidelity measures, and qubit counts. This expansion in hardware has been paralleled by a correspondingly rapid development of algorithms for quantum chemistry simulations, which are increasingly being implemented and tested on these emerging quantum computational systems.

Since the original proposal of using the quantum phase estimation (QPE)[9, 10] approach to estimate ground state energies of molecules, researchers have developed even more efficient implementations, through advances such as

* zhao@ionq.co

[†] shinkj@hyundai.com

qubitization[11, 12] and to leverage factorization methods such as tensor hypercontraction[13]. Using these algorithms, researchers have provided numerous estimates of the resources[8, 14, 15], such as compute time and number of qubits, required to solve some of the hardest chemical problems exactly with a fault-tolerant quantum computer.

Although resource estimation for fault-tolerant quantum computing is crucial to the development of the field, broadly accessible (and useful) fault-tolerant quantum computers are likely many years away. Currently, quantum devices operate within the era of noisy intermediate scale quantum (NISQ)[16, 17] computing. In the NISQ era, quantum computers face limitations in the number of utilizable qubits and the fidelity of quantum gates. For example, the Aria quantum computer developed by IonQ has 25 qubits with a two-qubit gate fidelity of 99.4%. Despite the high fidelity, the chance of error remains nonzero and this limits the number of operations that can be performed reliably on QPUs. This in turn limits the design and application of quantum algorithms. Developing algorithms that are noise-resilient on NISQ systems has drawn significant attention, and remains of utmost importance in the near-term. For chemistry, one NISQ algorithm that is particularly promising is the variational quantum eigensolver (VQE)[18–23] and its variants. VQE utilizes parametrized quantum circuits, known as ansätze, to estimate electronic wave functions. It employs the variational principle to optimize these parameters so as to locate the energy minimum. This minimum represents the optimal approximation of the exact wave function, within the limits of the parametrized circuit. VQE offers users the choice of an ansatz to strike a balance between accuracy and fidelity. Simpler ansätze lead to more efficient, shallower circuits, which are amenable to NISQ systems. However, they may lack the expressiveness to capture accurate chemical behaviors. Conversely, complex ansätze can improve accuracy, but their effectiveness is often diminished by noise as a consequence of compounding numerous qubit operations. Therefore, given a certain number of qubits and gate fidelities, users must carefully design VQE circuits to strike a balance between accuracy and fidelity. The potential quantum advantage of VQE is that it allows the efficient utilization of ansätze that are inefficient to compute classically, such as the unitary coupled cluster (UCC) ansatz,[18, 19, 24–26]. The UCC class of ansätze is known to offer more accurate energy predictions to its classical (projective) counterpart, especially for strongly correlated systems. However, as with the classical case, care must be given to the design and selection of the UCC-based ansatz depending on the chemical case at hand.

We recently developed a resource-efficient VQE algorithm[27] for quantum chemistry simulations. This algorithm takes advantage of the unitary pair coupled cluster doubles (upCCD)[28–30] ansatz. In the upCCD ansatz, all the electrons are paired, which allows each electron pair to be treated as an effective (hard-core) bosonic particle. Computationally, this allows one to map spatial orbitals to individual qubits. In doing so, the number of qubits required are reduced by half compared to the conventional Jordan-Wigner mapping of spin orbitals to qubits. In previous work, we demonstrated that the upCCD ansatz yields highly efficient

circuits with a constant overhead for energy measurements. We further showed that the orbital optimization (oo) effects, which are crucial for modeling bond breaking scenarios, could be applied to the upCCD circuit for no additional quantum cost, in the sense that there is no increase in either the circuit depth or the number of measurements beyond the additional macro-iterations for the orbital optimization loop. Preliminary results from using the oo-upCCD ansatz on IonQ’s trapped-ion quantum computer show that the predicted relative energies are in excellent agreements with a noiseless quantum simulator.

Despite this progress, it is worth noting that the oo-upCCD ansatz is not able to produce quantitative levels of accuracy, except for two-electron problems. The main reason is that it restricts the electrons to pairs, and the (generally significant) correlation energy contribution from broken-pair excitations is ignored. How one could account for the broken-pairs for oo-upCCD thus becomes a pressing issue. One obvious route is to implement these excitations using quantum circuits, but doing so one would immediately sacrifice two major advantages of the oo-upCCD ansatz: 1) the ability to only map spatial orbitals to qubits, and, 2) the constant energy measurement overhead. In addition, it would also drastically increase the circuit depth, even with the most optimal circuit compilation techniques.[31]

In this study, we pursue an alternative approach by first computing the reduced density matrices (RDMs) of the oo-upCCD circuits. From these RDMs, we leverage a second-order perturbation theory (PT2) framework to calculate the energetic contributions from broken-pair excitations. This method does not add to the circuit depth and maintains a constant energy measurement overhead. We apply this technique to model bond dissociation and chemical reactions using quantum simulators and IonQ’s trapped-ion quantum computers. Our objectives are twofold: to determine the accuracy achievable using oo-upCCD with a perturbative correction, as well as assess the performance of the perturbative algorithm on current quantum computing hardware.

The paper is structured as follows, we begin by introducing the oo-upCCD ansatz and its circuits. Then we dive into the second order perturbation theory and discuss the zeroth order Hamiltonian, the wave function correction, and derive the working equation for wave function and energy corrections. Having laid out the general formalism, we shift our attention to some of the numerical issues we face in the algorithms and some proposed solutions to it. Results are presented on quantum simulators and IonQ’s Aria and Forte quantum computers for potential energy surface predictions of N_2 , Li_2O , and two chemical reactions. We conclude with a summary of our findings and comments on future directions.

II. THEORY

A. The oo-upCCD Ansatz

The unitary pair coupled-cluster double (upCCD) ansatz is

$$|\Psi_{\text{upCCD}}\rangle = e^{T-T^\dagger} |\text{HF}\rangle \quad (1)$$

in which T is the pair-double cluster operator, defined as

$$T = \sum_{ia} t_i^a a_{a\alpha}^\dagger a_{a\beta}^\dagger a_{i\beta} a_{i\alpha} \quad (2)$$

in which i and a are indices for occupied and unoccupied orbitals in the HF state. $a_{p\alpha}^\dagger$ ($a_{p\beta}^\dagger$) and $a_{p\alpha}$ ($a_{p\beta}$) are the fermionic creation and annihilation operators in the p -th spin-up (α) or spin-down (β) orbital.

The exponentiation of the pair-excitation operator can be efficiently implemented with the following circuit, given in Figure 1,

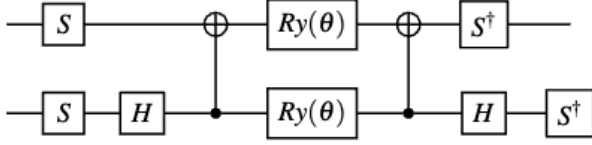


FIG. 1: A quantum circuit that implements the Givens rotation.

Once the circuit is defined, one needs to measure the energy expectation value $\langle \Psi_{\text{upCCD}} | H | \Psi_{\text{upCCD}} \rangle$ for the second-quantized Hamiltonian H . In the full electronic Hamiltonian, there are $O(N^4)$ terms in H , for which N is the number of qubits. However, due to pair symmetry, a majority of them do not contribute to the energy in the upCCD approximation. After eliminating these pair-breaking terms, one finds that only three measurements are needed (in the X , Y , and Z basis, respectively) to compute the energy. Moreover, the number of basis measurements are independent of problem size, and three circuits are all that is needed for *any* upCCD calculation.

One potential concern is that the upCCD ansatz defined in Equation 1 is not invariant to the choice of underlying orbitals. Previous studies [28, 30, 32, 33] on similar wave functions have found that it is necessary to optimize the orbitals along with the cluster amplitudes, especially for strongly correlated systems. The orbital optimized upCCD ansatz is

$$|\Psi_{\text{oo-upCCD}}\rangle = e^K e^{T-T^\dagger} |\text{HF}\rangle \quad (3)$$

in which there are two different sets of parameters: 1) circuit parameters in the cluster operator T , and, 2) orbital rotation parameters in the the orbital rotation operator K , which is defined as

$$K = \sum_{p>q} \sum_{\sigma} K_{pq} (a_{p\sigma}^\dagger a_{q\sigma} - a_{q\sigma}^\dagger a_{p\sigma}) \quad (4)$$

Here K is an anti-Hermitian matrix and σ indexes the spin.

B. The VQE Perturbation Theory

As mentioned previously, the cluster operator in upCCD does not contain any broken-pair excitations. By neglecting

these terms, we observe a quantitative deviation from the exact energy. To remedy this, we would like to recover the energetic corrections from these terms. To account for the broken-pair contributions we use perturbation theory as follows. We first write the molecular Hamiltonian as

$$H = H_0 + \lambda V \quad (5)$$

in which H_0 is a simple non-interacting Hamiltonian and V accounts for the electron interaction. λ is the scale of the interaction.

We then write the energy and wave function in terms of λ

$$\begin{aligned} |\Psi\rangle &= |\Psi^{(0)}\rangle + \lambda |\Psi^{(1)}\rangle + \lambda^2 |\Psi^{(2)}\rangle + \dots \\ E &= E^{(0)} + \lambda E^{(1)} + \lambda^2 E^{(2)} + \dots \end{aligned} \quad (6)$$

Plugging the wave function and energy into the time-independent Schrodinger's equation, and selecting terms up to second order in λ , we obtain

$$\begin{aligned} H_0 |\Psi^{(0)}\rangle &= E^{(0)} |\Psi^{(0)}\rangle \\ H_0 |\Psi^{(1)}\rangle + V |\Psi^{(0)}\rangle &= E^{(0)} |\Psi^{(1)}\rangle + E^{(1)} |\Psi^{(0)}\rangle \\ H_0 |\Psi^{(2)}\rangle + V |\Psi^{(1)}\rangle &= E^{(0)} |\Psi^{(2)}\rangle + E^{(1)} |\Psi^{(1)}\rangle + E^{(2)} |\Psi^{(0)}\rangle \end{aligned} \quad (7)$$

Next, we constrain $|\Psi^{(1)}\rangle$ such that it is orthogonal to $|\Psi^{(0)}\rangle$

$$\langle \Psi^{(1)} | \Psi^{(0)} \rangle = 0. \quad (8)$$

After left projecting Equation 7 by $\langle \Psi^{(0)} |$, we obtain

$$\begin{aligned} \langle \Psi^{(0)} | H_0 | \Psi^{(0)} \rangle &= E^{(0)} \\ \langle \Psi^{(0)} | V | \Psi^{(0)} \rangle &= E^{(1)} \\ \langle \Psi^{(0)} | V | \Psi^{(1)} \rangle &= E^{(2)} \end{aligned} \quad (9)$$

For our reference (zeroth-order) wave function, $|\Psi^{(0)}\rangle$, we can use the oo-pUCCD wave function obtained by oo-VQE:

$$|\Psi^{(0)}\rangle = |\Psi_{\text{oo-upCCD}}\rangle \quad (10)$$

We then partition the second-quantized molecular Hamiltonian as

$$H = \sum_p \varepsilon_p a_p^\dagger a_p + \sum_{pq} h_{pq} a_p^\dagger a_q + \sum_{pqrs} g_{pqrs} a_p^\dagger a_q^\dagger a_r a_s \quad (11)$$

and we define the zeroth order Hamiltonian as

$$H_0 = \sum_p \varepsilon_p a_p^\dagger a_p \quad (12)$$

in which where p runs over all spin orbitals and ε_p are the orbital energies computed by plugging the one body reduced

density matrix (1-RDM) of oo-upCCD into the HF orbital energy expression. Similarly, we define the perturbation potential V as

$$V = \sum_{pq} h_{pq} a_p^\dagger a_q + \sum_{pqrs} g_{pqrs} a_p^\dagger a_q a_r^\dagger a_s. \quad (13)$$

The VQE energy on its own contains both the zeroth and first order energy corrections

$$E_{\text{VQE}} = E^{(0)} + E^{(1)}. \quad (14)$$

The leading energy correction beyond the VQE energy enters in the second order

$$\begin{aligned} E_{\text{VQE}} &= E^{(0)} + E^{(1)} = \langle \Psi^{(0)} | H_0 | \Psi^{(0)} \rangle + \langle \Psi^{(0)} | V | \Psi^{(0)} \rangle \\ &= \langle \Psi^{(0)} | H_0 + V | \Psi^{(0)} \rangle \\ &= \langle \Psi^{(0)} | H | \Psi^{(0)} \rangle. \end{aligned} \quad (15)$$

Let's now write the first-order wave function correction as

$$|\Psi^{(1)}\rangle = \sum_{pqrs}^{\text{non-pair}} t_{pqrs} a_p^\dagger a_q a_r^\dagger a_s |\Psi^{(0)}\rangle = \sum_P^{\text{non-pair}} t_P |\Psi_P\rangle \quad (16)$$

in which $a_p^\dagger a_q a_r^\dagger a_s$ breaks electron pairs.

In order for $a_p^\dagger a_q a_r^\dagger a_s$ to break electron pairs, we must consider these three scenarios

$$\begin{aligned} &a_{p\alpha}^\dagger a_{q\alpha} a_{r\alpha}^\dagger a_{s\alpha} (r \neq s, p \neq q, r \neq q, s \neq p) (p < r, q < s) \\ &a_{p\beta}^\dagger a_{q\beta} a_{r\beta}^\dagger a_{s\beta} (r \neq s, p \neq q, r \neq q, s \neq p) (p < r, q < s) \quad (17) \\ &a_{p\alpha}^\dagger a_{q\alpha} a_{r\beta}^\dagger a_{s\beta} (r \neq s, p \neq q, p \neq r | |q \neq s) \end{aligned}$$

in which the first parenthesis enforces broken-pairing, and the second parenthesis ensures no double counting.

The second-order energy correction becomes

$$E^{(2)} = \sum_P^{\text{non-pair}} t_P \langle \Psi^{(0)} | V | \Psi_P \rangle \quad (18)$$

in which we need to compute t_P .

Left projecting Equation 7 by $|\Psi_Q\rangle$, we obtain

$$\sum_P t_P \langle \Psi_Q | H_0 | \Psi_P \rangle + \langle \Psi_Q | V | \Psi^{(0)} \rangle = E^{(0)} \sum_P t_P \langle \Psi_Q | \Psi_P \rangle \quad (19)$$

where both P and Q denote non-pair excitations. Rearranging the above equation gives:

$$\begin{aligned} \sum_P t_P \left(\langle \Psi_Q | H_0 | \Psi_P \rangle - E^{(0)} \langle \Psi_Q | \Psi_P \rangle \right) &= - \langle \Psi_Q | V | \Psi^{(0)} \rangle \\ \sum_P G_{PQ} t_P &= -Y_Q \end{aligned} \quad (20)$$

where we define

$$\begin{aligned} G_{PQ} &= \langle \Psi_Q | H_0 | \Psi_P \rangle - E^{(0)} \langle \Psi_Q | \Psi_P \rangle \\ Y_P &= \langle \Psi_P | V | \Psi^{(0)} \rangle \end{aligned} \quad (21)$$

so we can then solve \vec{t} by

$$\vec{t} = -\mathbf{G}^{-1} \vec{Y}. \quad (22)$$

We then plug \vec{t} into Equation 18 to compute $E^{(2)}$. Finally, the total energy is

$$E = E_{\text{VQE}} + E^{(2)} \quad (23)$$

Now we need to compute the \mathbf{G} matrix and the \vec{Y} vector. Elements of the \mathbf{G} matrix take the form

$$\begin{aligned} G_{PQ} &= \sum_k \varepsilon_k \left\langle \Psi^{(0)} | a_u^\dagger a_v a_x^\dagger a_y a_k^\dagger a_k a_p^\dagger a_q a_r^\dagger a_s | \Psi^{(0)} \right\rangle \\ &\quad - E^{(0)} \left\langle \Psi^{(0)} | a_u^\dagger a_v a_x^\dagger a_y a_p^\dagger a_q a_r^\dagger a_s | \Psi^{(0)} \right\rangle \end{aligned} \quad (24)$$

We approximate \mathbf{G} with its diagonal elements

$$\begin{aligned} G_{PP} &= \sum_k \varepsilon_k \left\langle \Psi^{(0)} | a_s^\dagger a_r a_q^\dagger a_p a_k^\dagger a_k a_p^\dagger a_q a_r^\dagger a_s | \Psi^{(0)} \right\rangle \\ &\quad - E^{(0)} \left\langle \Psi^{(0)} | a_s^\dagger a_r a_q^\dagger a_p a_p^\dagger a_q a_r^\dagger a_s | \Psi^{(0)} \right\rangle \\ &= \sum_k \varepsilon_k \Gamma_{sqkpr}^{rpkqs} - E^{(0)} \Gamma_{sqpr}^{rpkqs} \end{aligned} \quad (25)$$

in which we have defined the 5-particle reduced density matrix (5-RDM).

We also need to compute the \vec{Y} vector as

$$\begin{aligned} Y_P &= \sum_{pq} h_{pq} \left\langle \Psi^{(0)} | a_u^\dagger a_v a_x^\dagger a_y a_p^\dagger a_q | \Psi^{(0)} \right\rangle \\ &\quad + \sum_{pqrs} g_{pqrs} \left\langle \Psi^{(0)} | a_u^\dagger a_v a_x^\dagger a_y a_p^\dagger a_q a_r^\dagger a_s | \Psi^{(0)} \right\rangle \\ &= \sum_{pq} h_{pq} \Gamma_{uxp}^{vypq} + \sum_{pqrs} g_{pqrs} \Gamma_{uxpr}^{vypqs} \end{aligned} \quad (26)$$

in which we need 3- and 4-RDMs. h and g are the one- and two-electron integrals, respectively.

The most computationally-intensive step of the VQE-PT2 approach is in the computation of the 4-RDMs from Equation 26, which contains eight different indices. However, although the term $a_p^\dagger a_q a_r^\dagger a_s |\Psi^{(0)}\rangle$ in the first-order wave function correction contains broken-pair configurations, all electrons should still be paired in $a_u^\dagger a_v a_x^\dagger a_y a_p^\dagger a_q a_r^\dagger a_s |\Psi^{(0)}\rangle$. Otherwise the overlap with $|\Psi^{(0)}\rangle$ becomes zero. Therefore, only four indices out of the original eight are unique, and the operator $a_u^\dagger a_v a_x^\dagger a_y a_p^\dagger a_q a_r^\dagger a_s$ must be written in terms of

- number operators $n_p = a_p^\dagger a_p \rightarrow \frac{1}{2}(1 - Z_p)$
- double creation operators $d_p^\dagger = a_{p\alpha}^\dagger a_{p\beta}^\dagger \rightarrow \frac{1}{2}(X_p - iY_p)$
- double annihilation operators $d_p = a_{p\beta} a_{p\alpha} \rightarrow \frac{1}{2}(X_p + iY_p)$

in which the expression at the right of the arrow is the Jordan-Wigner transformed formalism of these operators.

Therefore, for 4-RDMs, one only needs to measure a subset of rank-4 Pauli strings that includes: 1) Pauli strings with

four Pauli-Z matrices, 2) Pauli strings with two Pauli-Z matrices and two Pauli-X matrices, 3) Pauli strings with two Pauli-Z matrices and two Pauli-Y matrices, 4) Pauli strings with two Pauli-X matrices and two Pauli-Y matrices. The rest of the Pauli strings do not contribute as a result of symmetry violation. We then group this Pauli strings and find terms that are qubitwise commutative[34] with each other, and measure them altogether. A detailed description of how to construct the 4-RDMs efficiently can be found in the Supplementary Information.

C. Regularization

The perturbation theory described in previous sections may run into numerical instability issues without regularization. The numerical instability arises from two reasons. First, if a broken-pair excitation in the wave function corrections excites an electron from (to) a nearly empty (occupied) orbital, then both G and Y would be small and their division in Equation 22 would be unstable. Second, since oo-upCCD includes orbital optimization effects, in bond breaking scenarios, the HOMO-LUMO gap closes as one stretches the bond, which also reduces the magnitude of G and leads to numerical instability.

In order to tackle this problem, we take the same approach of the orbital optimized Møller-Plesset second order perturbation theory (ooMP2)[35, 36] and add a regularization to the amplitude, which becomes

$$t_p = -\frac{Y_p}{G_{pp}}(1 - e^{-\sigma G_{pp}}) \quad (27)$$

in which we introduce an empirical parameter σ that controls the strength of the regularization.

As one could see, if $G = 0$, then the regularized t_p also becomes zero and it no longer contributes to the wave function. In the regularized ooMP2, σ is obtained by fitting to a known database, and the optimal σ is found to be 1.5. In our case, we use a much larger σ , which is chosen to be 28. Such a large σ allows us to completely remove the numerical instability that arises when G is close to zero, while it only damps little correlation energy away when G is far away from zero. In the future, a more appropriate scheme for choosing σ may be to fit to a known dataset. However, optimal selection of σ is beyond the scope of the present study.

III. COMPUTATIONAL DETAILS

The oo-upCCD circuits are implemented in the Qiskit software platform,[37] and all the simulator results are obtained from the statevector simulator provided by Qiskit. The full configuration interaction (FCI) and the complete active space configuration interaction (CASCI) results were obtained from PySCF[38] package. The Li, O, C, and N $1s$ orbitals are frozen at the restricted Hartree-Fock (RHF) level. For Br and I atoms, all the non-valence orbitals are frozen at the RHF level. The oo-upCCD circuit parameter optimization is performed with the L-BFGS optimization technique. All

the calculations are performed using the minimal STO-3G basis. Error bars on the potential energy surface plots represent \pm one standard error as a result of finite sampling. The molecular geometries along the reaction path for CH_2OH^+ decomposition were taken from intrinsic reaction coordinate calculation[39]. The molecular structures along the minimum energy path of $\text{S}_{\text{N}}2$ reaction of $\text{CH}_3\text{I} + \text{Br}^-$ were obtained using the nudged elastic band method[40–42].

The experimental demonstration was performed on the Aria and Forte quantum processing units (QPUs) developed by IonQ. Both QPUs utilize trapped Ytterbium ions where two states in the ground hyperfine manifold are used as qubit states. These states are manipulated by illuminating individual ions with pulses of 355 nm light that drive Raman transitions between the ground states defining the qubit. By configuring these pulses, arbitrary single qubit gates and Mølmer-Sørensen type two-qubit gates can both be realized. The Forte system[43] contains larger qubit registers and improved gate fidelities than Aria due to the acoustic-optic deflectors that allow independent alignment of each laser beam to each ion. This technique leads to smaller beam alignment error across the chain of trapped ions.

IV. RESULTS

A. N_2

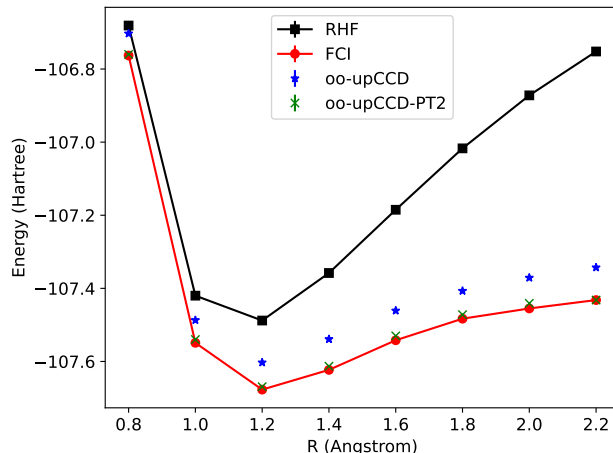


FIG. 2: Potential energy surface for the dissociation of the N_2 molecule in the STO-3G basis computed with RHF, oo-upCCD, oo-upCCD-PT2, and FCI. VQE results are obtained from a noise-free simulator.

We begin our numerical results with the dissociation of the N_2 triple bond. In Figure 2, we compare the energy predicted by RHF, oo-upCCD, oo-upCCD-PT2, and FCI. We observe that the oo-upCCD energy provides a significant improvement over RHF, but it remains far from the FCI energy. This is due to the missing of broken-pair excitation contributions in the oo-upCCD wave function. After applying the perturbation correction, we find that it is now much closer to FCI.

The nonparallelity error (NPE) defined as the difference between the largest and smallest error with respect to FCI along the potential surface, is reduced from 52mH to 14mH, which demonstrates the effectiveness of the perturbation correction.

B. Li_2O

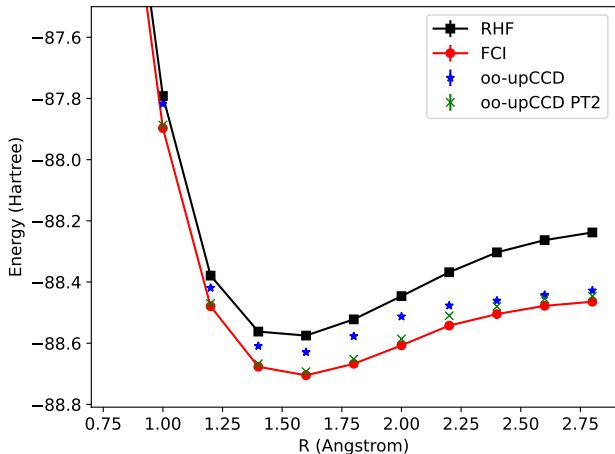


FIG. 3: Potential energy surface for the symmetric dissociation of the Li_2O molecule in the STO-3G basis computed with RHF, oo-upCCD, oo-upCCD-PT2, and FCI. VQE results are obtained from a noise-free simulator.

Our second example is the symmetric dissociation of the Li_2O molecule. Li_2O is one of the secondary reaction products in lithium-air batteries, which is a potential candidate for next-generation lithium battery due to its high energy density. The results on an ideal simulator are shown in Figure 3, comparing RHF, FCI, oo-upCCD, and oo-upCCD-PT2. As one could see, similar to the N_2 dissociation, the oo-upCCD-PT2 significantly improves the accuracy of oo-upCCD, and reduces the NPE v.s. FCI from 69mH to 24mH. This is particularly true in the equilibrium geometry. When bonds are stretched, oo-upCCD-PT2 still exhibits some noticeable amount of errors compared to FCI. These remaining errors are due to the limitation of the chosen form of the second order perturbation theory, such as 1) higher order terms are needed 2) one needs to use a different zeroth-order Hamiltonian than the simple one-body one we use. 3) the diagonal approximation of the G matrix.

C. Chemical Reactions

1. Results on Simulator

We now move our attention to the chemical decomposition process of the $\text{CH}_2\text{OH}^+ \rightarrow \text{HCO}^+ + \text{H}_2$ and the $\text{S}_{\text{N}}2$ reaction $\text{CH}_3\text{I} + \text{Br}^- \rightarrow \text{CH}_3\text{Br} + \text{I}^-$. The simulated energy profile along the reaction path is shown in Figure 4 for the CH_2OH^+ decomposition. After freezing the core orbitals, the remaining eleven spatial molecular orbitals are mapped to eleven

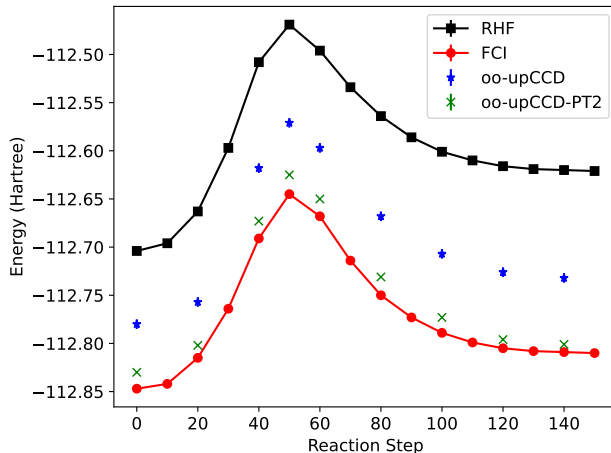


FIG. 4: The simulated $\text{CH}_2\text{OH}^+ \rightarrow \text{HCO}^+ + \text{H}_2$ reaction energy pathway using RHF, oo-upCCD, oo-upCCD-PT2, and FCI. VQE results are obtained from a noise-free simulator.

qubits. Unsurprisingly, oo-upCCD without perturbative corrections is insufficient to produce quantitative accuracy for absolute energies, capturing roughly only 50% of correlation energy. However, due to error cancellation, the predicted reaction energy barrier (209 mH) is close to FCI (202 mH). The energy difference between reactants and products (ΔE) is predicted to be 50 mH by oo-upCCD, which overestimates the FCI prediction (38 mH) by 24%. Applying the PT2 correction significantly improves the results, and we are able to capture 88% of the correlation. The predicted reaction energy barrier and ΔE is 205 mH and 39 mH respectively, which reduces the original oo-upCCD error by 57% and 92%.

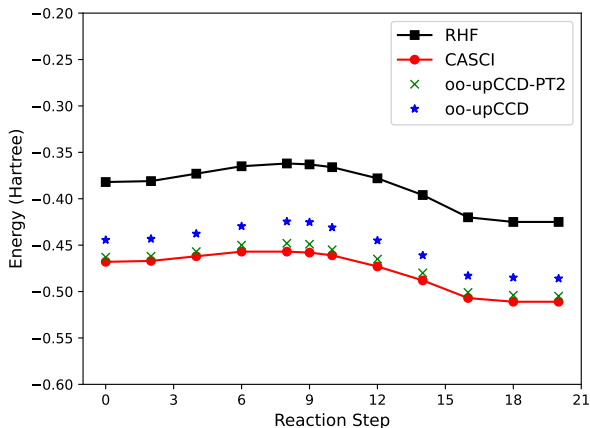


FIG. 5: The simulated $\text{CH}_3\text{I} + \text{Br}^- \rightarrow \text{CH}_3\text{Br} + \text{I}^-$ $\text{S}_{\text{N}}2$ reaction reaction energy pathway using RHF, oo-upCCD, oo-upCCD-PT2, and FCI. VQE results are obtained from a noise-free simulator. Energies are offset by 9434 Hartree for legibility.

The simulated results of the $\text{S}_{\text{N}}2$ reaction of $\text{CH}_3\text{I} + \text{Br}^-$ are shown in Figure 5. After freezing the core orbitals, we

end up with 15 spatial orbitals/qubits to simulate. We now use the CASCI simulations in the same active space as references. Similar to the CH_2OH^+ decomposition, the perturbation correction brings the oo-upCCD energy much closer to the CASCI predictions. Besides absolute energies, relative energies are also improved. The predicted barrier height is 14 mH by oo-upCCD-PT2 v.s. 10 mH by CASCI, which reduces the error of oo-upCCD (19 mH) by 50%.

2. Results on IonQ Quantum Computer

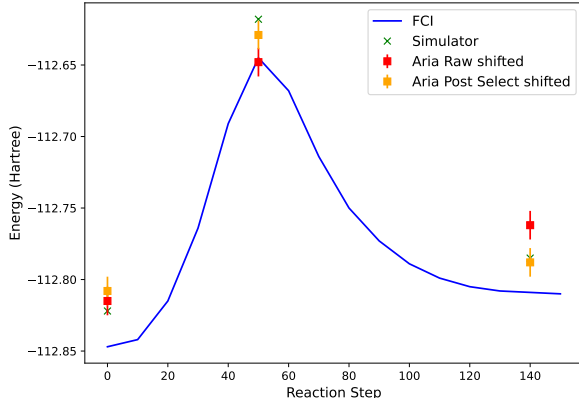


FIG. 6: The simulated $\text{CH}_2\text{OH}^+ \rightarrow \text{HCO}^+ + \text{H}_2$ reaction energy pathway on the IonQ Aria quantum computer.

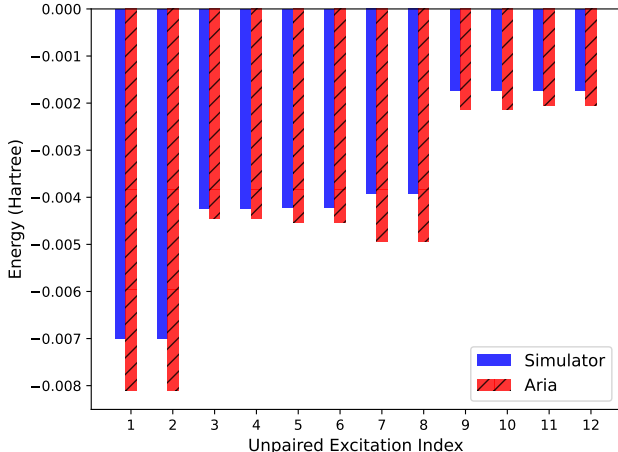


FIG. 7: The energy contribution to $E^{(2)}$ from the top 12 unpaired excitations for reaction step 140 of the CH_2OH^+ decomposition, comparing the statevector simulator and the Aria QPU.

Motivated by the success of perturbation theory for oo-upCCD in quantum simulators, we performed these chemical reaction simulations on two generations of the IonQ’s quantum computers. We simulate reaction steps 0, 50, and 140 of

TABLE I: Energy contributions of oo-upCCD-PT2 for CH_2OH^+ between the ideal simulator and the Aria QPU.

System	E_{VQE} (sim)	E_{VQE} (Aria)	$E^{(2)}$ (sim)	$E^{(2)}$ (Aria)
Reactant	-112.822	-112.400	-0.048	-0.051
Transition State	-112.565	-112.228	-0.053	-0.057
Product	-112.726	-112.332	-0.059	-0.067

TABLE II: Energy contributions of oo-upCCD-PT2 for the $\text{S}_{\text{N}}2$ reaction between the ideal simulator and the Forte QPU.

System	E_{VQE} (sim)	E_{VQE} (Forte)	$E^{(2)}$ (sim)	$E^{(2)}$ (Forte)
Reactant	-9434.463	-9434.014	-0.018	-0.019
Transition State	-9434.449	-9433.976	-0.023	-0.023
Product	-9434.505	-9433.967	-0.019	-0.019

the CH_2OH^+ decomposition process on the Aria QPU. These three points correspond to the reactants, transition state, and products, respectively. We first perform a circuit pruning process, in which gates whose parameters are below a chosen threshold are removed from the circuit. In our experience, the minor energy benefits derived from these small-parameter quantum operations are overshadowed by the introduction of system noise. In our study, we choose the threshold to be 0.04 radians. The pruned circuits have 10 CX gates and 46 single qubit gates. The experimental results are shown in Figure 6. As expected, the introduction of hardware noise yields a systematic, positive bias to the total energy. However, after we shift the data points by a constant (364 mH), the experimental results roughly match the prediction of the noiseless simulator. This suggests that the hardware errors are consistent across reaction steps and the relative energy is not affected.

The total energy of oo-upCCD-PT2 contains two parts: the oo-upCCD energy (E_{VQE}) and the energy correction ($E^{(2)}$). Table I shows the energy contributions from these two parts comparing the statevector simulator and the Aria QPU, and we find that almost all the errors in energy are from the oo-upCCD energy term. This could be understood in two ways. First, the magnitude of the oo-upCCD energy is much larger than the energy correction, and so with the same error rate, the former would result in larger absolute errors than the latter. Second, the perturbative energy correction also benefits from the error cancellation, as the errors in the numerator (Y_p^2) and the denominator (G_p) may cancel with each other. Therefore, the energy correction appears significantly more resilient to errors than the oo-upCCD energy. In Figure 7 we plot the energy contribution to $E^{(2)}$ from unpaired excitations whose Y_p/G_p^2 are above 1 mH, comparing the predictions of the statevector simulator and the Aria QPU. Clearly, the predictions from Aria are in excellent agreement with the simulator.

In order to improve the absolute energy measurements of oo-upCCD, we take advantage of a simple error mitigation approach based on post selection. For the Z-basis measurements, only measurements that preserve particle number symmetry are kept, and the rest are discarded. The results are shown in Figure 6. We find that doing so improves the en-

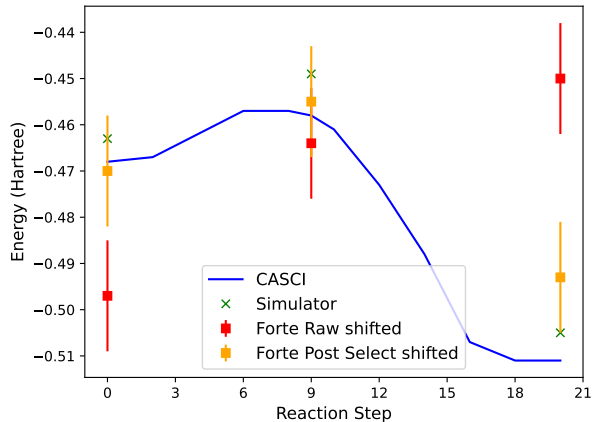


FIG. 8: The simulated $\text{CH}_3\text{I} + \text{Br}^- \rightarrow \text{CH}_3\text{Br} + \text{I}^-$ $\text{S}_{\text{N}}2$ reaction energy pathway on the IonQ Forte quantum computer. Energies are offset by 9434 Hartree for legibility.

ergy measurements by about 200 mH. We then perform the uniform shift for the post-selected energies by 151 mH, and the results better match the results from the ideal simulator. This demonstrates that the post-selection not only improves absolute energies, but also relative energies.

The experimental results of the $\text{CH}_3\text{I} + \text{Br}^-$ $\text{S}_{\text{N}}2$ reaction are shown in Figure 8 and Table II. These results are obtained using the IonQ Forte QPU. The $\text{S}_{\text{N}}2$ reaction of $\text{CH}_3\text{I} + \text{Br}^-$ is particularly challenging for NISQ quantum systems as the energy differences across the reaction path are small. The energy difference between the transition state and the reactant is about 50 mH, which is a value on the order of the experimental uncertainty. As seen in Figure 8, the raw energy demonstrates nonphysical behavior. That is, the product energy is even higher than the transition state and the reactant energies. Similar to the CH_2OH^+ decomposition, the error in the total energy is predominantly due to errors from the unperturbed VQE energy. Therefore, we apply the same Z-basis post selection, and find that the error mitigated energies now yield the correct behavior, matching well with the predictions of the simulator and CASCI.

V. CONCLUSION

A common question regarding current NISQ quantum computers is their utility for quantum chemistry, particularly for electronic structure problems. To address this, accurate simulations on these systems are essential. However, considering the VQE algorithm as an example, many proposed VQE algorithms—based on unitary coupled cluster ansatz or hardware-efficient ansatz,[20, 44–47] still produce circuits that are beyond the capabilities of today’s quantum computers, except for very small chemical systems. The oo-upCCD ansatz is arguably the most practical VQE variant for execution on contemporary quantum computers for chemical systems. Its benefits are threefold: first, it requires only half the qubits compared to many existing VQE ansätze. Second,

the scaling of two-qubit gates with system size is quadratic ($O(N^2)$) with respect to system size. Finally, the number of necessary circuits to execute remains constant ($O(1)$), regardless of the system size.

Our goal in this study was to explore ways to enhance the precision of the oo-upCCD method while keeping the complexity of the quantum circuit the same (or increasing it in a shallow, controlled manner). Here, we investigated the use of RDM-based second-order perturbation theory. Our findings indicate that this technique can correct most of the errors caused by the electron-pair assumptions of oo-upCCD, especially during the dissociation of multiple bonds in nitrogen (N_2) and lithium oxide (Li_2O) molecules, as well as in calculating the energy barriers and differences between reactants and products in chemical reactions. Trials conducted on IonQ’s trapped-ion quantum computers demonstrate that the energy corrections predicted by PT2 are robust against noise, which can be attributed to the cancellation of errors within the PT2 energy formula. This characteristic suggests that it can be an effective method for use in the current generation of quantum computers.

Despite its advantages, the oo-upCCD-PT2 method faces challenges similar to those found in traditional perturbation theory, including numerical instability and variational collapse. We intend to tackle these challenges in future research. By continuing to refine our methods, in conjunction with hardware improvements, we aim to develop a practical VQE algorithm for near-term devices. This algorithm is intended to solve complex chemical problems with accuracy equal to or surpassing current classical simulation methods. We anticipate that the outcomes of these experiments will offer critical insights into the utility of near-term QPUs for quantum chemistry.

In summary, we have effectively leveraged RDM-based methods to refine the accuracy of the oo-upCCD method through second-order perturbation theory. We demonstrated this through successful applications on both quantum simulators and actual quantum hardware. Motivated by these initial positive results, in future work, we plan to address some of the issues associated with the perturbation theory. A primary issue we observed is the violation of the variational principle, notably during the dissociation of nitrogen (N_2). This limitation may be overcome by implementing measurements within the framework of configuration interaction rather than perturbation theory, potentially leading to an approach similar to the quantum subspace expansion (QSE). In addition to QSE, the recently developed non-orthogonal quantum eigensolver (NOQE)[48] also provides with a useful platform for quantum chemistry simulations beyond VQE, although the Hadamard test used in NOQE will increase the circuit complexity. We plan to explore these and more directions with the goal of landing us on practical quantum advantage for quantum chemistry simulations.

VI. DATA AVAILABILITY

The data presented in this manuscript are available from the corresponding author upon reasonable request.

ACKNOWLEDGMENTS

We thank the Hyundai Motor Company for funding this research through the Hyundai-IonQ Joint Quantum Computing Research Project. We thank Melanie Hiles for running the experiments on QPUs. We thank Dr. Seung Hyun Hong, and Dr. Jongkook Lee at Hyundai Motor Company for enlightening discussions.

AUTHOR CONTRIBUTIONS

L. Z, K.S., and W. K. conceived of the project. L.Z., J.G., Q. W., and K. S. designed, implemented, and evaluated the algorithms. Experimental data were collected and analyzed by L. Z. and K. S.; All authors contributed to drafting and editing the manuscript.

COMPETING INTERESTS

The authors declare no competing interests.

- [1] Y. Cao, J. Romero, J. P. Olson, M. Degroote, P. D. Johnson, M. Kieferová, L. D. Kivlichan, T. Menke, B. Peropadre, N. P. D. Sawaya, S. Sim, L. Veis, and A. Aspuru-Guzik, “Quantum Chemistry in the Age of Quantum Computing,” *Chem. Rev.* **119**, 10856–10915 (2019).
- [2] E. Farhi, J. Goldstone, and S. Gutmann, “A Quantum Approximate Optimization Problem,” arXiv preprint arXiv:1411.4028v1 (2014).
- [3] M. Benedetti, E. Lloyd, S. Sack, and M. Fiorentini, “Parametrized Quantum Circuits as Machine Learning Models,” *Quantum Sci. Technol.* **4**, 043001 (2019).
- [4] Attila Szabo and Neil S. Ostlund, *Modern Quantum Chemistry: Introduction to Advanced Electronic Structure Theory* (Dover Publications, Mineola, N.Y., 1996).
- [5] B. Bauer, S. Bravyi, M. Motta, and G. K-L. Chan, “Quantum Algorithms for Quantum Chemistry and Quantum Materials Science,” *Chem. Rev.* **120**, 12685–12717 (2020).
- [6] J. E. Rice, T. P. Gujarati, M. Motta, T. Y. Takeshita, E. Lee, J. A. Latone, and J. M. Garcia, “Quantum Computation of Dominant Products in Lithium–Sulfur Batteries,” *J. Chem. Phys.* **154**, 134115 (2021).
- [7] N. S. Blunt, J. Camps, O. Crawford, R. Izsák, S. Leontica, A. Mirani, A. E. Moylett, S. A. Scivier, C. Sünderhauf, P. Schopf, J. M. Taylor, and N. Holzmann, “A Perspective on the Current State-of-the-Art of Quantum Computing for Drug Discovery Applications,” *J. Chem. Theory Comput.* **18**(12), 7001–7023 (2022).
- [8] V. von Burg, G. H. Low, T. Häner, D. S. Steiger, M. Reiher, M. Roetteler, and M. Troyer, “Quantum Computing Enhanced Computational Catalysis,” *Phys. Rev. Research* **3**, 033055 (2021).
- [9] A. Aspuru-Guzik, A. D. Dutoi, P. J. Love, and M. Head-Gordon, “Simulated Quantum Computation of Molecular Energies,” *Science* **309**, 1704–1707 (2005).
- [10] B. P. Lanyon, J. D. Whitfield, G. G. Gillett, M. E. Goggin, M. P. Almeida, I. Kassal, J. D. Biamonte, M. Mohseni, B. J. Powell, M. Barbieri, A. Aspuru-Guzik, and A. G. White, “Towards Quantum Chemistry on a Quantum Computer,” *Nat. Chem.* **2**, 106–111 (2010).
- [11] G. H. Low and I. L. Chuang, “Hamiltonian Simulation by Qubitization,” *Quantum* **3**, 163 (2019).
- [12] R. Babbush, C. Gidney, D. W. Berry, N. Wiebe, J. McClean, A. Paler, A. Fowler, and H. Neven, “Encoding Electronic Spectra in Quantum Circuits with Linear T Complexity,” *Phys. Rev. X* **8**, 041015 (2018).
- [13] J. Lee, D. W. Berry, C. Gidney, W. J. Huggins, J. R. McClean, N. Wiebe, and R. Babbush, “Even More Efficient Quantum Computations of Chemistry Through Tensor Hypercontraction,” *PRX Quantum* **2**, 030305 (2021).
- [14] M. Reiher, N. Wiebe, K. M. Svore, D. Wecker, and M. Troyer, “Elucidating Reaction Mechanisms on Quantum Computers,” *Proc. Natl. Acad. Sci. U.S.A.* **114**, 7555–7560 (2017).
- [15] N. S. Blunt, J. Camps, O. Crawford, R. Izsák, S. Leontica, A. Mirani, A. E. Moylett, S. A. Scivier, C. Sünderhauf, P. Schopf, J. M. Taylor, and N. Holzmann, “Perspective on the Current State-of-the-Art of Quantum Computing for Drug Discovery Applications,” *J. Chem. Theory Comput.* **18**, 7001–7023 (2022).
- [16] J. Preskill, “Quantum Computing in the NISQ era and beyond,” *Quantum* **2**, 79 (2018).
- [17] K. Bharti, A. Cervera-Lierta, T. H. Kyaw, T. Hang, S. Alperin-Lea, A. Anand, M. Degroote, H. Heimonen, J. S. Kottmann, T. Menke, W-K. Mok, S. Sim, L-C. Kwek, and A. Aspuru-Guzik, “Noisy Intermediate-Scale Quantum (NISQ) Algorithms,” *Rev. Mod. Phys.* **94**, 015004 (2022).
- [18] A. Peruzzo, J. McClean, P. Shadbolt, M-H. Yung, X-Q. Zhou, P. J. Love, A. Aspuru-Guzik, and J. O’Brien, “A Variational Eigenvalue Solver on a Photonic Quantum Processor,” *Nat. Commun.* **5**, 5213 (2014).
- [19] P. J. J. O’Malley, R. Babbush, I. D. Kivlichan, J. Romero, J. R. McClean, and et al, “Scalable Quantum Simulation of Molecular Energies,” *Phys. Rev. X* **6**, 031007 (2016).
- [20] A. Kandala, A. Mezzacapo, K. Temme, M. Takita, M. Brink, J. M. Chow, and J. M. Gambetta, “Hardware-Efficient Variational Quantum Eigensolver for Small Molecules and Quantum Magnets,” *Nature* **549**, 242–246 (2017).
- [21] Google AI Quantum and Collaborators, “Hartree-Fock on a Superconducting Qubit Quantum Computer,” *Science* **369**, 1084–1089 (2020).
- [22] Y. Nam, J-S. Chen, N. C. Pimenti, K. Wright, C. Delaney, D. Maslov, K. R. Brown, S. Allen, J. M. Amini, J. Apisdorf, K. M. Beck, A. Blinov, V. Chaplin, M. Chmielewski, C. Collins, S. Debnath, K. M. Hudek, A. M. Ducore, M. Keesan, S. M. Kreikemeier, J. Mizrahi, P. Solomon, M. Williams, J. D. Wong-Campos, D. Moehring, C. Monroe, and J. Kim, “Ground-State Energy Estimation of the Water Molecule on a Trapped-Ion Quantum Computer,” *npj Quantum Information* **6**, 33 (2020).
- [23] Q. Wang, M. Li, C. Monroe, and Y. Nam, “Resource-Optimized Fermionic Local-Hamiltonian Simulation on a Quantum Computer for Quantum Chemistry,” Preprint at <https://doi.org/10.22331/q-2021-07-26-509> (2021).
- [24] H. R. Grimsley, D. Claudino, S. E. Economou, E. Barnes, and N. J. Mayhall, “Is the Trotterized UCCSD Ansatz Chemically Well-Defined?” *J. Chem. Theory Comput.* **16**, 1–6 (2020).
- [25] H. R. Grimsley, S. E. Economou, E. Barnes, and N. J. Mayhall, “An Adaptive Variational Algorithm for Exact Molecular Simulations on a Quantum Computer,” *Nat. Commun.* **10**, 3007 (2019).
- [26] A. J. McCaskey, Z. P. Parks, J. Jakowski, S. V. Moore, T. D. Morris, T. S. Humble, and R. C. Pooser, “Quantum Chemistry as a Benchmark for Near-Term Quantum Computers,” *npj Quantum Information* **5**, 99 (2019).
- [27] L. Zhao, J. Goings, K. Wright, J. Nguyen, J. Kim, S. Johri, K. Shin, W. Kyoung, J. I. Fuks, J-K. K. Rhee, and Y. M. Rhee, “Orbital-Optimized Pair-Correlated Electron Simulations on Trapped-Ion Quantum Computers,” *npj Quantum Information* **9** (2023).
- [28] I. O. Sokolov, P. KI. Barkoutsos, P. J. Ollitrault, D. Greenberg, J. Rice, M. Pistoia, and I. Tavernelli, “Quantum Orbital-Optimized Unitary Coupled Cluster Methods in the Strongly Correlated Regime: Can Quantum Algorithms Outperform Their Classical Equivalents?” *J. Chem. Phys.* **152**, 124107 (2020).
- [29] T. E. O’Brien and et al, “Purification-based Quantum Error Mitigation of Pair-Correlated Electron Simulations,” *Nat. Phys.* (2023).
- [30] L. Zhao and E. Neuscamman, “Amplitude Determinant Coupled Cluster with Pairwise Doubles,” *J. Chem. Theory Comput.* **12**, 5841–5850 (2016).
- [31] J. Goings, L. Zhao, J. Jakowski, T. Morris, and R. Pooser, “Molecular Symmetry in VQE: A Dual Approach for Trapped-Ion Simulations of Benzene,” Preprint at <https://doi.org/10.48550/arXiv.2308.00667> (2023).

- [32] P. A. Limacher, T. D. Kim, P. W. Ayers, P. A. Johnson, S. D. Baerdemacker, D. Van Neck, and P. Bultinck, "The Influence of Orbital Rotation on the Energy of Closed-Shell Wavefunctions," *Mol. Phys.* **112**, 853–862 (2014).
- [33] T. M. Henderson, I. W. Bulik, and G. E. Scuseria, "Pair Extended Coupled Cluster Doubles," *J. Chem. Phys.* **142**, 214116 (2015).
- [34] P. Gokhale, O. Angiuli, Y. Ding, K. Gui, T. Tomesh, M. Suchara, M. Martonosi, and F. T. Chong, "Minimizing State Preparations in Variational Quantum Eigensolver by Partitioning into Commuting Families," arXiv preprint, arXiv:1907.13623v1 (2019).
- [35] "Regularized Orbital-Optimized Second-Order Møller-Plesset Perturbation Theory: A Reliable Fifth-Order-Scaling Electron Correlation Model with Orbital Energy Dependent Regularizers," *J. Chem. Theory Comput.* **14**(10), 5203–5219 (2018).
- [36] "Regularized Second-Order Møller-Plesset Theory: A More Accurate Alternative to Conventional MP2 for Noncovalent Interactions and Transition Metal Thermochemistry for the Same Computational Cost," *J. Chem. Theory Comput.* **12**(50), 12084–12097 (2021).
- [37] Qiskit contributors, "Qiskit: An Open-Source Framework for Quantum Computing," (2023).
- [38] Qiming Sun, Timothy C. Berkelbach, Nick S. Blunt, George H. Booth, Sheng Guo, Zhendong Li, Junzi Liu, James D. McClain, Elvira R. Sayfutyarova, Sandeep Sharma, Sebastian Wouters, and Garnet Kin Lic Chan, "PySCF: the Python-Based Simulations of Chemistry Framework," *Wiley Interdiscip. Rev. Comput. Mol. Sci.* **8** (2018).
- [39] Y. M. Rhee and M. S. Kim, "Dynamic Isotope Effect on the Product Energy Partitioning in $\text{CH}_2\text{OH}^{\rightarrow}\text{CHO}^++\text{H}_2$," *J. Chem. Phys.* **109**, 5363 (1998).
- [40] G. Henkelman, B. P. Uberuaga, and H. Jónsson, "A Climbing Image Nudged Elastic Band Method for Finding Saddle Points and Minimum Energy Paths," *J. Chem. Phys.* **113**, 9901–9904 (2000).
- [41] G. Henkelman and H. Jónsson, "Improved Tangent Estimate in the Nudged Elastic Band Method for Finding Minimum Energy Paths and Saddle Points," *J. Chem. Phys.* **113**, 9978–9985 (2000).
- [42] D. Sheppard, R. Terrell, and G. Henkelman, "Optimization Methods for Finding Minimum Energy Paths," *J. Chem. Phys.* **128**, 134106 (2008).
- [43] J-S. Chen, E. Nielsen, M. Ebert, V. Inlek, K. Wright, V. Chaplin, A. Maksymov, E. Páez, A. Poudel, P. Maunz, and J. Gamble, "Benchmarking a Trapped-Ion Quantum Computer with 29 Algorithmic Qubits," Preprint at <https://doi.org/10.48550/arXiv.2308.05071> (2023).
- [44] P. Kl. Barkoutsos, J. F. Gonthier, I. Sokolov, N. Moll, G. Salis, A. Fuhrer, M. Ganzhorn, D. J. Egger, M. Troyer, A. Mezzacapo, S. Filipp, and I. Tavernelli, "Quantum Algorithms for Electronic Structure Calculations: Particle-Hole Hamiltonian and Optimized Wave-Function Expansions," *Phys. Rev. A* **98**, 022322 (2018).
- [45] I. G. Ryabinkin, T-C. Yen, S. N. Genin, and A. F. Izmaylov, "Qubit Coupled Cluster Method: A Systematic Approach to Quantum Chemistry on a Quantum Computer," *J. Chem. Theory Comput.* **14**, 6317–6326 (2018).
- [46] I. G. Ryabinkin, R. A. Lang, S. N. Genin, and A. F. Izmaylov, "Iterative Qubit Coupled Cluster Approach with Efficient Screening of Generators," *J. Chem. Theory Comput.* **16**, 1055–1063 (2020).
- [47] G-L. R. Anselmetti, D. Wierichs, C. Gogolin, and R. M. Parrish, "Local, Expressive, Quantum-Number-Preserving VQE ansätze for Fermionic Systems," *New J. Phys.* **23**, 113010 (2021).
- [48] U. Baek, D. Hait, J. Shee, O. Leimkuhler, W. J. Huggins, T. F. Stetina, M. Head-Gordon, and K. B. Whaley, "Say NO to Optimization: A Nonorthogonal Quantum Eigensolver," *PRX Quantum* **4**, 030307 (2023).

Supplementary Information: Enhancing the Electron Pair Approximation with Measurements on Trapped Ion Quantum Computers

Luning Zhao* and Joshua Goings
IonQ Inc, College Park, MD, 20740, USA

Qingfeng Wang
Chemical Physics Program and Institute for Physical Science and Technology,
University of Maryland, College Park, MD, 20742, USA

Kyuji Shin,[†] Woomin Kyoung, and Seunghyo Noh
Materials Research & Engineering Center, CTO Division,
Hyundai Motor Company, Uiwang 16082, Republic of Korea

Young Min Rhee and Kyungmin Kim
Department of Chemistry, KAIST, Daejeon, 34141, Republic of Korea
(Dated: December 12, 2023)

S1. CONSTRUCTION OF 4RDM

In the implementation of the pair-VQE, the Hamiltonian is written as

$$\begin{aligned}
 H = & \sum_{pq} g_{pq} \left(a_{p\alpha}^\dagger a_{q\alpha} + a_{p\beta}^\dagger a_{q\beta} \right) \\
 & + \sum_{pqrs} (pq|rs) \left(\frac{1}{2} a_{p\alpha}^\dagger a_{q\alpha} a_{r\alpha}^\dagger a_{s\alpha} + \frac{1}{2} a_{p\beta}^\dagger a_{q\beta} a_{r\beta}^\dagger a_{s\beta} \right) \\
 & + \sum_{pqrs} (pq|rs) a_{p\alpha}^\dagger a_{q\alpha} a_{r\beta}^\dagger a_{s\beta}
 \end{aligned} \tag{S1}$$

in which g is the modified one-electron integrals

$$g_{pq} = h_{pq} - \frac{1}{2} \sum_r (pr|rq) \tag{S2}$$

and $(pq|rs)$ is the usual two-electron coulomb integrals in (11|22) order.

Therefore, for 4-RDMs, there are three different categories.

$$\begin{aligned}
 & \langle \Psi^{(0)} | a_{u\alpha}^\dagger a_{v\alpha} a_{x\alpha}^\dagger a_{y\alpha} a_{p\alpha}^\dagger a_{q\alpha} a_{r\alpha}^\dagger a_{s\alpha} | \Psi^{(0)} \rangle \\
 & \langle \Psi^{(0)} | a_{u\alpha}^\dagger a_{v\alpha} a_{x\alpha}^\dagger a_{y\alpha} a_{p\beta}^\dagger a_{q\beta} a_{r\beta}^\dagger a_{s\beta} | \Psi^{(0)} \rangle \\
 & \langle \Psi^{(0)} | a_{u\alpha}^\dagger a_{v\alpha} a_{x\alpha}^\dagger a_{y\alpha} a_{p\alpha}^\dagger a_{q\alpha} a_{r\beta}^\dagger a_{s\beta} | \Psi^{(0)} \rangle
 \end{aligned} \tag{S3}$$

For each category, there are three sub-categories, which corresponds to $\alpha\alpha$, $\beta\beta$, and $\alpha\beta$ excitations. For example,

$$\begin{aligned}
 & \langle \Psi^{(0)} | a_{u\alpha}^\dagger a_{v\alpha} a_{x\alpha}^\dagger a_{y\alpha} a_{p\alpha}^\dagger a_{q\alpha} a_{r\alpha}^\dagger a_{s\alpha} | \Psi^{(0)} \rangle (x < u, y < v, u \neq v, x \neq y, u \neq y, v \neq x) \\
 & \langle \Psi^{(0)} | a_{u\beta}^\dagger a_{v\beta} a_{x\beta}^\dagger a_{y\beta} a_{p\alpha}^\dagger a_{q\alpha} a_{r\alpha}^\dagger a_{s\alpha} | \Psi^{(0)} \rangle (x < u, y < v, u \neq v, x \neq y, u \neq y, v \neq x) \\
 & \langle \Psi^{(0)} | a_{u\alpha}^\dagger a_{v\alpha} a_{x\beta}^\dagger a_{y\beta} a_{p\alpha}^\dagger a_{q\alpha} a_{r\alpha}^\dagger a_{s\alpha} | \Psi^{(0)} \rangle (u \neq v, x \neq y, x \neq u || y \neq v)
 \end{aligned} \tag{S4}$$

* zhao@ionq.co

[†] shinkj@hyundai.com

As one could see, the first term can only contain 4 number operators to be non-zero. The second term can only contain 2 pair-double excitation operators. The third term can contain 2 number operators and one pair-double excitation operator.

Take the first term for example, there are only 4 possible cases for this term to be non-zero.

$$\begin{aligned}
 u &= q, v = p, x = s, y = r \\
 u &= s, v = p, x = q, y = r \\
 u &= q, v = r, x = s, y = p \\
 u &= s, v = r, x = q, y = p
 \end{aligned}
 \tag{S5}$$

For second term, the possible cases are

$$\begin{aligned}
 u &= p, v = q, x = r, y = s \\
 u &= r, v = q, x = p, y = s \\
 u &= p, v = s, x = r, y = q \\
 u &= r, v = q, x = p, y = s
 \end{aligned}
 \tag{S6}$$

Here we show how to build the 4RDM constructively. The problem is defined as the following.

$$\left\langle \Psi^{(0)} | a_u^\dagger a_v a_x^\dagger a_y a_p^\dagger a_q a_r^\dagger a_s | \Psi^{(0)} \right\rangle
 \tag{S7}$$

where $u, v, x, y, p, q, r, s \in \{0, 1, \dots, 2n - 1\}$ indicating spin orbitals where n is the number of molecular orbitals. The indices u, v, x, y has the following additional constraints:

1. (u, v) and (x, y) must belongs to the same spin respectively
2. $u > x, v > y$
3. As generalized excitation term, u, v, x, y must not belong to same spin orbital, but they can be in the same molecular orbital of different spins
4. $a_u^\dagger a_v a_x^\dagger a_y$ must break the pair symmetry
5. $a_u^\dagger a_v a_x^\dagger a_y a_p^\dagger a_q a_r^\dagger a_s$ must conserve the pair symmetry

Since for each valid tuple of $(uvxy)$, there must be at least one valid $(pqrs)$ but not vise versa, it is more efficient to enumerate all valid $(uvxy)$ and derive its corresponding valid $(pqrs)$. All valid types of $(uvxy)$ are shown in Fig. S1 . For example, for (1) in Fig. S1, it means out of all molecular orbitals, choose four of them and assign the α spin part of the molecular orbital to $(uvxy)$. Notice, however, when enumerate all possible $(uvxy)$, it still needs to satisfy the additional condition that $x < u, y < v$.

For each of the above cases, we need to derive a matching $(pqrs)$ so that the combined eight indices sill preserve the symmetry. We showed all possible combinations of $(uvxy)$ and $(pqrs)$ in Fig. 2.

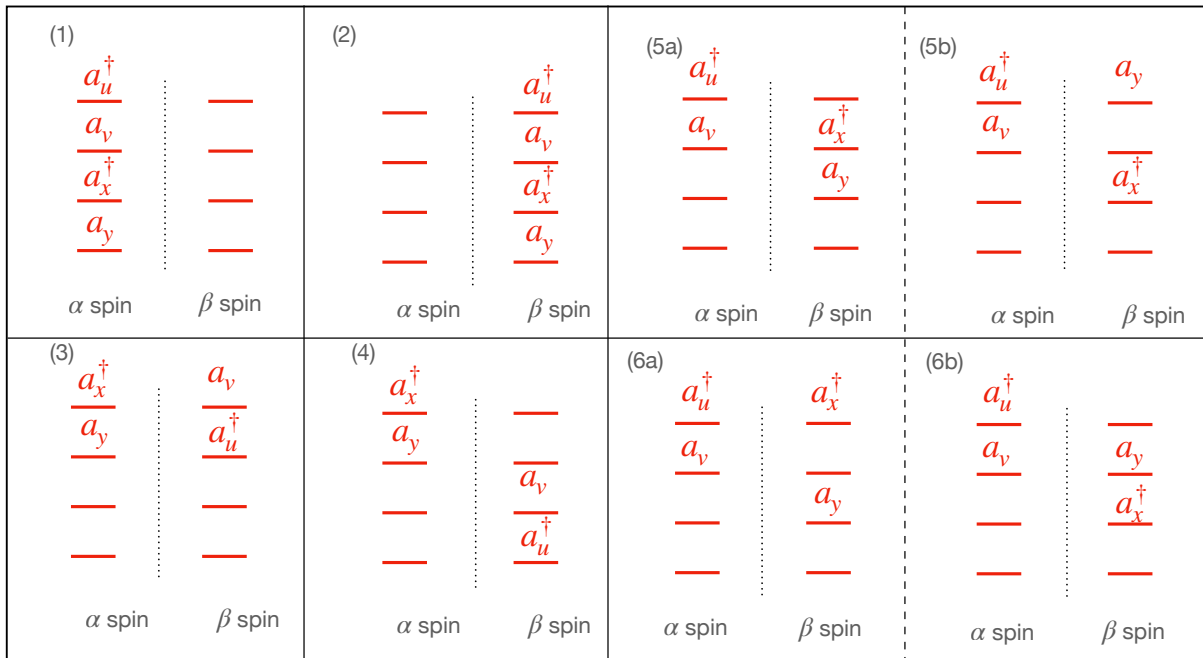


FIG. S1: All possible index combinations for $(uvxy)$ that breaks paired symmetry. The four levels corresponds to arbitrarily chosen four molecular orbitals among all possible molecular orbitals. The two bars on the same level corresponds to the two spin orbitals of the same molecular orbital. The spin types of $(uvxy)$ are described as the following. (1) $\alpha\alpha\alpha\alpha$ on different molecular orbitals. (2) $\beta\beta\beta\beta$ on different molecular orbitals. (3) $\alpha\alpha\beta\beta$ on two molecular orbitals. (4) $\alpha\alpha\beta\beta$ on four different molecular orbitals. (5) $\alpha\alpha\beta\beta$ on three molecular orbitals with (5a) annihilation-creation operators share the same molecular orbital or (5b) creation-annihilation operators share the same molecular orbital. (6) $\alpha\alpha\beta\beta$ on three molecular orbitals with (6a) two creation operators share the same molecular orbital or (6b) two annihilation operators share the same molecular orbital.

Case 1	$\begin{array}{c} a_u^\dagger a_q \\ a_v a_p^\dagger \\ a_x^\dagger a_s \\ a_y a_r^\dagger \end{array}$ α spin β spin	$\begin{array}{c} a_u^\dagger a_q \\ a_v a_p^\dagger \\ a_x^\dagger a_s \\ a_y a_r^\dagger \end{array}$ α spin β spin	$\begin{array}{c} a_u^\dagger a_q \\ a_v a_p^\dagger \\ a_x^\dagger a_s \\ a_y a_r^\dagger \end{array}$ α spin β spin	$\begin{array}{c} a_u^\dagger a_q \\ a_v a_p^\dagger \\ a_x^\dagger a_s \\ a_y a_r^\dagger \end{array}$ α spin β spin	$\begin{array}{c} a_u^\dagger a_q \\ a_v a_p^\dagger \\ a_x^\dagger a_s \\ a_y a_r^\dagger \end{array}$ α spin β spin	$\begin{array}{c} a_u^\dagger a_q \\ a_v a_p^\dagger \\ a_x^\dagger a_s \\ a_y a_r^\dagger \end{array}$ α spin β spin	$\begin{array}{c} a_u^\dagger a_q \\ a_v a_p^\dagger \\ a_x^\dagger a_s \\ a_y a_r^\dagger \end{array}$ α spin β spin	
Case 2	$\begin{array}{c} a_u^\dagger a_q \\ a_v a_p^\dagger \\ a_x^\dagger a_s \\ a_y a_r^\dagger \end{array}$ α spin β spin	$\begin{array}{c} a_u^\dagger a_q \\ a_v a_p^\dagger \\ a_x^\dagger a_s \\ a_y a_r^\dagger \end{array}$ α spin β spin	$\begin{array}{c} a_u^\dagger a_q \\ a_v a_p^\dagger \\ a_x^\dagger a_s \\ a_y a_r^\dagger \end{array}$ α spin β spin	$\begin{array}{c} a_u^\dagger a_q \\ a_v a_p^\dagger \\ a_x^\dagger a_s \\ a_y a_r^\dagger \end{array}$ α spin β spin	$\begin{array}{c} a_u^\dagger a_q \\ a_v a_p^\dagger \\ a_x^\dagger a_s \\ a_y a_r^\dagger \end{array}$ α spin β spin	$\begin{array}{c} a_u^\dagger a_q \\ a_v a_p^\dagger \\ a_x^\dagger a_s \\ a_y a_r^\dagger \end{array}$ α spin β spin	$\begin{array}{c} a_u^\dagger a_q \\ a_v a_p^\dagger \\ a_x^\dagger a_s \\ a_y a_r^\dagger \end{array}$ α spin β spin	$\begin{array}{c} a_u^\dagger a_q \\ a_v a_p^\dagger \\ a_x^\dagger a_s \\ a_y a_r^\dagger \end{array}$ α spin β spin
Case 4	$\begin{array}{c} a_x^\dagger a_s \\ a_y a_r^\dagger \\ a_u^\dagger a_q \\ a_v a_p^\dagger \end{array}$ α spin β spin	$\begin{array}{c} a_x^\dagger a_s \\ a_y a_r^\dagger \\ a_u^\dagger a_q \\ a_v a_p^\dagger \end{array}$ α spin β spin	$\begin{array}{c} a_x^\dagger a_s \\ a_y a_r^\dagger \\ a_u^\dagger a_q \\ a_v a_p^\dagger \end{array}$ α spin β spin	$\begin{array}{c} a_x^\dagger a_s \\ a_y a_r^\dagger \\ a_u^\dagger a_q \\ a_v a_p^\dagger \end{array}$ α spin β spin	$\begin{array}{c} a_x^\dagger a_s \\ a_y a_r^\dagger \\ a_u^\dagger a_q \\ a_v a_p^\dagger \end{array}$ α spin β spin	$\begin{array}{c} a_x^\dagger a_s \\ a_y a_r^\dagger \\ a_u^\dagger a_q \\ a_v a_p^\dagger \end{array}$ α spin β spin	$\begin{array}{c} a_x^\dagger a_s \\ a_y a_r^\dagger \\ a_u^\dagger a_q \\ a_v a_p^\dagger \end{array}$ α spin β spin	$\begin{array}{c} a_x^\dagger a_s \\ a_y a_r^\dagger \\ a_u^\dagger a_q \\ a_v a_p^\dagger \end{array}$ α spin β spin
Index for case 1,2,4	$(p, r) = P(v, y)$ $(q, s) = P(u, x)$	$(p, r) = P(v, X)$ $(q, s) = P(u, Y)$	$(p, r) = P(X, y)$ $(q, s) = P(u, V)$	$(p, r) = P(U, v)$ $(q, s) = P(x, Y)$	$(p, r) = P(U, y)$ $(q, s) = P(V, x)$	$(p, r) = P(U, X)$ $(q, s) = P(V, Y)$		
Case 3	$\begin{array}{c} a_x^\dagger a_s \\ a_y a_r^\dagger \\ a_u^\dagger a_q \\ a_v a_p^\dagger \end{array}$ α spin β spin	$(p, r) = P(v, y)$ $(q, s) = P(u, x)$	$\begin{array}{c} a_x^\dagger a_s \\ a_y a_r^\dagger \\ a_u^\dagger a_q \\ a_v a_p^\dagger \end{array}$ α spin β spin	$(p, r) = P(v, v)$ $(q, s) = P(u, u)$	$\begin{array}{c} a_x^\dagger a_s \\ a_y a_r^\dagger \\ a_u^\dagger a_q \\ a_v a_p^\dagger \end{array}$ α spin β spin	$(p, r) = P(y, y)$ $(q, s) = P(x, x)$		
Case 5a	$\begin{array}{c} a_u^\dagger a_q \\ a_v a_p^\dagger \\ a_x^\dagger a_s \\ a_y a_r^\dagger \end{array}$ α spin β spin	$(p, r) = P(v, y)$ $(q, s) = P(u, x)$	$\begin{array}{c} a_u^\dagger a_q \\ a_v a_p^\dagger \\ a_x^\dagger a_s \\ a_y a_r^\dagger \end{array}$ α spin β spin	$(p, r) = P(v, U)$ $(q, s) = P(x, Y)$	$\begin{array}{c} a_u^\dagger a_q \\ a_v a_p^\dagger \\ a_x^\dagger a_s \\ a_y a_r^\dagger \end{array}$ α spin β spin	$(p, r) = P(v, v)$ $(q, s) = P(u, Y)$	$\begin{array}{c} a_u^\dagger a_q \\ a_v a_p^\dagger \\ a_x^\dagger a_s \\ a_y a_r^\dagger \end{array}$ α spin β spin	$(p, r) = P(U, y)$ $(q, s) = P(x, x)$
Case 5b	$\begin{array}{c} a_u^\dagger a_p^\dagger \\ a_v a_q \\ a_x^\dagger a_s \\ a_y a_r^\dagger \end{array}$ α spin β spin	$(p, r) = P(v, y)$ $(q, s) = P(u, x)$	$\begin{array}{c} a_u^\dagger a_p^\dagger \\ a_v a_q \\ a_x^\dagger a_s \\ a_y a_r^\dagger \end{array}$ α spin β spin	$(p, r) = P(X, y)$ $(q, s) = P(u, V)$	$\begin{array}{c} a_u^\dagger a_p^\dagger \\ a_v a_q \\ a_x^\dagger a_s \\ a_y a_r^\dagger \end{array}$ α spin β spin	$(p, r) = P(y, y)$ $(q, s) = P(V, x)$	$\begin{array}{c} a_u^\dagger a_p^\dagger \\ a_v a_q \\ a_x^\dagger a_s \\ a_y a_r^\dagger \end{array}$ α spin β spin	$(p, r) = P(v, X)$ $(q, s) = P(u, u)$
Case 6a	$\begin{array}{c} a_u^\dagger a_p^\dagger \\ a_v a_q \\ a_x^\dagger a_s \\ a_y a_r^\dagger \end{array}$ α spin β spin	$(p, r) \in P(v, i)$ $(q, s) \in P(Y, i)$ For $i \in$ all spin orbitals	$\begin{array}{c} a_u^\dagger a_p^\dagger \\ a_v a_q \\ a_x^\dagger a_s \\ a_y a_r^\dagger \end{array}$ α spin β spin	$(p, r) \in P(v, i)$ $(q, s) \in P(V, i)$ For $i \in$ all spin orbitals	$\begin{array}{c} a_u^\dagger a_p^\dagger \\ a_v a_q \\ a_x^\dagger a_s \\ a_y a_r^\dagger \end{array}$ α spin β spin	$(p, r) \in P(v, y)$ $(q, s) \in P(i, i + N_{\text{mo}})$ For $i \in$ all molecular orbitals and $i \neq Y$ (to skip the duplicate in 6a.1.) $i \neq v$ (to skip the duplicate in 6a.2)	$\begin{array}{c} a_u^\dagger a_p^\dagger \\ a_v a_q \\ a_x^\dagger a_s \\ a_y a_r^\dagger \end{array}$ α spin β spin	$(p, r) \in P(i, i + N_{\text{mo}})$ $(q, s) \in P(V, Y)$ For $i \in$ all molecular orbitals and $i \neq v$ (to skip the duplicate in 6a.1.) $i \neq Y$ (to skip the duplicate in 6a.2)
Case 6b	$\begin{array}{c} a_u^\dagger a_p^\dagger \\ a_v a_q \\ a_x^\dagger a_s \\ a_y a_r^\dagger \end{array}$ α spin β spin	$(p, r) \in P(U, i)$ $(q, s) \in P(x, i)$ For $i \in$ all spin orbitals	$\begin{array}{c} a_u^\dagger a_p^\dagger \\ a_v a_q \\ a_x^\dagger a_s \\ a_y a_r^\dagger \end{array}$ α spin β spin	$(p, r) \in P(X, i)$ $(q, s) \in P(u, i)$ For $i \in$ all spin orbitals	$\begin{array}{c} a_u^\dagger a_p^\dagger \\ a_v a_q \\ a_x^\dagger a_s \\ a_y a_r^\dagger \end{array}$ α spin β spin	$(p, r) \in P(U, X)$ $(q, s) \in P(i, i + N_{\text{mo}})$ For $i \in$ all molecular orbitals and $i \neq X$ (to skip the duplicate in 6b.1.) $i \neq u$ (to skip the duplicate in 6b.2)	$\begin{array}{c} a_u^\dagger a_p^\dagger \\ a_v a_q \\ a_x^\dagger a_s \\ a_y a_r^\dagger \end{array}$ α spin β spin	$(p, r) \in P(i, i + N_{\text{mo}})$ $(q, s) \in P(u, x)$ For $i \in$ all molecular orbitals and $i \neq u$ (to skip the duplicate in 6b.1.) $i \neq X$ (to skip the duplicate in 6b.2)

FIG. S2: The figure lists the rules to generate valid indices for $\langle \Psi^{(0)} | a_u^\dagger a_v a_x^\dagger a_y a_p^\dagger a_q a_r^\dagger a_s | \Psi^{(0)} \rangle$ for a given $a_u^\dagger a_v a_x^\dagger a_y$. All indices are spin orbital indices. $P(\cdot, \cdot)$ represents the permutation function to generate valid indices and is defined as $P(x, y) = \begin{cases} \{(x, y), (y, x)\} & \text{if } x \neq y \\ \{(x, x)\} & \text{if } x = y \end{cases}$. The capitalization of the letter indicates a index of opposite spin. For example, $U = u + N_{\text{mo}}$ if u is α spin and $U = u - N_{\text{mo}}$ if u is β spin, where N_{mo} is the number of molecular orbitals. For example, for all three cases (case 1, 2 and 4) in the first column, the (p, r) should be $P(v, y) = \{(v, y), (y, v)\}$ which means $p = v, r = y$ or $p = y, r = v$, while (q, s) should be $P(u, x) = \{(u, x), (x, u)\}$. So the valid operators are $a_u^\dagger a_v a_x^\dagger a_y a_p^\dagger a_q a_r^\dagger a_s$, $a_u^\dagger a_v a_x^\dagger a_y a_p^\dagger a_x a_r^\dagger a_s$, $a_u^\dagger a_v a_x^\dagger a_y a_p^\dagger a_q a_r^\dagger a_u$, $a_u^\dagger a_v a_x^\dagger a_y a_p^\dagger a_x a_r^\dagger a_u$, $a_u^\dagger a_v a_x^\dagger a_y a_p^\dagger a_q a_r^\dagger a_u$.

S2. EFFICIENT POST-PROCESSING

In this section we explain another major effort to improve the speed for evaluating the expectation value of second-quantized Hamiltonians that satisfy pair-symmetry. Since the second quantized operator O_J to be measured satisfies the pair symmetry, it can always be partitioned as

$$O_J = \prod_{jk} a_j^\dagger a_k \rightarrow (-1)^b \prod_{jk} a_{j\alpha}^\dagger a_{j\beta}^\dagger a_{k\alpha} a_{k\beta} \prod_l a_l^\dagger a_l \prod_m a_m a_m^\dagger \quad (\text{S8})$$

that is, paired excitation parts, and number operator parts. We then expand the fermionic operators with the following transformation

$$a_{j\alpha}^\dagger a_{j\beta}^\dagger = \frac{1}{2}(X_j - iY_j) \quad (\text{S9})$$

$$a_{j\alpha} a_{j\beta} = -\frac{1}{2}(X_j + iY_j) \quad (\text{S10})$$

$$a_l^\dagger a_l = \frac{1}{2}(I - Z_l) \quad (\text{S11})$$

$$a_l a_l^\dagger = \frac{1}{2}(I + Z_l) \quad (\text{S12})$$

and take only the real part. So each of the

$$O_J = \prod_{jk} a_j^\dagger a_k \mapsto \sum_j h_j \otimes_k \sigma_v^{(jk)} = \sum_j h_j P_j \quad (\text{S13})$$

where $\sigma_v \in \{I, X, Y, Z\}$ is one of the Pauli operators and P_j denotes a Pauli string. As a result, in order to obtain $\langle O_J \rangle$, we only need to obtain $\langle P_j \rangle$.

Notice there will be many P_j that are duplicates from different O_J . To avoid duplicate measurement and post-processing, we first collect all unique P_j from all $\{O_J\}$ of interest to form a set $\{P_j\}$, obtain $\{\langle P_j \rangle\}$ and store it into a hash table (such as dictionary in Python). Then to recover the $\langle O_J \rangle$, we only need to retrieve the $\langle P_j \rangle$ from $\{\langle P_j \rangle\}$ and then sum them up with the weight h_j in each O_J . It is worth noting that, when measure the expectation value for $\{P_j\}$, we can measure several Paul strings simultaneously without the increase of the number of two-qubit gates as long as all Pauli strings to be measured simultaneously are mutually qubit-wise-commuting. In practice we use the qiskit qubit-wise-commuting function.